Feature Selection for Unsupervised Anomaly Detection and Localization Using Synthetic Defects

Lars Heckler[1,2] and Rebecca König[1]

[1] *MVTec Software GmbH, Germany*

[2] *Technical University of Munich, Germany*

Keywords: Anomaly Detection, Feature Selection, Visual Inspection, Synthetic Defects.

Abstract: Expressive features are crucial for unsupervised visual Anomaly Detection and Localization. State-of-the-art methods like PatchCore or SimpleNet heavily exploit such features from pretrained extractor networks and model their distribution or utilize them for training further parts of the model. However, the layers commonly used for feature extraction might not represent the optimal choice for reaching maximum performance. Thus, we present the first application-specific feature selection strategy for the task of unsupervised Anomaly Detection and Localization that identifies the most suitable layer of a pretrained feature extractor based on the performance on a synthetic validation set. The proposed selection strategy is applicable to any feature extraction-based AD method and may serve as a competitive baseline for future work by not only outperforming single-layer baselines but also features ensembled from multiple layer outputs.

1 INTRODUCTION

Detecting and localizing anomalies in natural images is an important task in modern computer vision. Anomalies manifest themselves in various ways such as structural defects (Bergmann et al., 2019a; Zou et al., 2022) or the violation of logical constraints (Bergmann et al., 2022). Consequently, the task of Anomaly Detection and Localization (AD) has a wide range of application areas reaching from the medical domain (Seeböck et al., 2020; Menze et al., 2015) over autonomous driving (Blum et al., 2019; Hendrycks et al., 2019) and video surveillance (Nazare et al., 2018; Li et al., 2013) to industrial inspection (Bergmann et al., 2019a; Zou et al., 2022). Especially within the industrial context AD depicts a crucial tool for quality assurance. Since modern production lines are highly automated and aim for maximum production quality it is difficult to acquire defective samples that can be used within the design phase of an AD system. Besides, all possible defect types that might occur for a product cannot be known prior to the launch of fabrication. For these reasons, the task of industrial AD is predominantly tackled in an unsupervised way, where the training of the AD method only requires anomaly-free samples.

Within the domain of unsupervised AD, methods that are built on top of pretrained networks have become popular. These pretrained networks such as ResNets (He et al., 2016) trained for ImageNet classification (Krizhevsky et al., 2012) are used for extracting features from the input images and stay frozen during both training and inference time. Here, the underlying assumption for solving the task of Anomaly Detection is that the feature extractor generates dis-

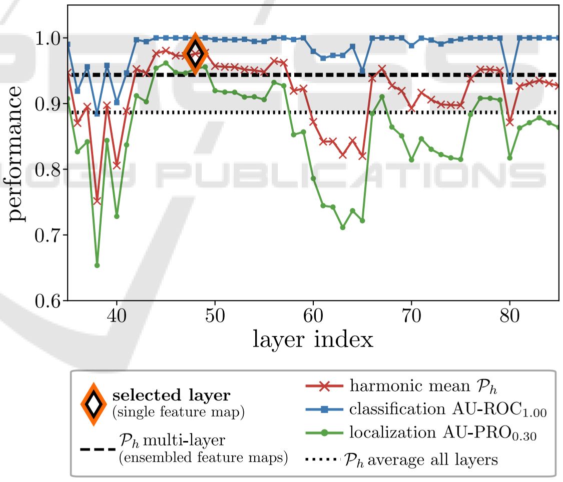

Figure 1: Application-specific feature selection for *PatchCore*. Performance of a layer is shown when exclusively utilizing its corresponding feature map from the feature extractor. Using the features of a single Wide ResNet-50 layer chosen by the proposed application-specific selection strategy can practically improve the harmonic mean $\mathcal{P}_h$ between anomaly classification and localization over several baselines, even over features ensembled from multiple layers, as shown here for MVTec AD object *tile*.

Heckler, L. and König, R.
Feature Selection for Unsupervised Anomaly Detection and Localization Using Synthetic Defects.
DOI: 10.5220/0012385500003660

In *Proceedings of the 19th International Joint Conference on Computer Vision, Imaging and Computer Graphics Theory and Applications (VISIGRAPP 2024) - Volume 3: VISAPP*, pages 154-165
ISBN: 978-989-758-679-8; ISSN: 2184-4321

tinct features for anomaly-free and anomalous images that can then be exploited to differentiate between these two classes. Moreover, extracting features on a local patch level might allow a precise localization of a defect (Roth et al., 2022; Defard et al., 2020).

Commonly, the extracted features originate from the same layers of the feature extractor for every application scenario. However, recently Heckler et al. (2023) systematically analyzed the importance of pretrained feature extractors for unsupervised AD and the corresponding choice of features. They found that existing state-of-the-art AD methods are highly sensitive to the particular choice of feature extractor and layer. In addition, the potential benefits in performance of using distinct feature layers for distinct application scenarios was highlighted. Motivated by these findings, we ask how to determine the features of a pretrained feature extractor that are most suitable for a specific AD task without requiring access to any real defective samples. The proposed feature selection strategy builds upon the generation of synthetic defects to estimate the suitability of a layer to provide expressive features for the given task. Extensive experiments demonstrate the effectiveness and feasibility of application-specific feature selection for Anomaly Detection and Localization, exemplarily shown in Figure 1. In particular, our key contributions are:

- We present the first feature selection strategy for the task of unsupervised Anomaly Detection and Localization that builds a competitive baseline for future work within this research direction.
- Applying the proposed selection strategy that does not require any real defective data we demonstrate that it is feasible to select the features of a single layer to obtain performances comparable or superior to feature ensembling approaches.
- By fine-grained experiments we confirm the importance of incorporating feature selection strategies into future method development since common choices of feature layers are not guaranteed to be optimal for a specific approach and application scenario.

2 RELATED WORK

As outlined by recent surveys (Liu et al., 2023a; Cui et al., 2023; Prunella et al., 2023), the task of Anomaly Detection and Localization can be tackled in various ways. Generally, Anomaly Detection methods can be separated into reconstruction-based and embedding-based methods. Reconstruction-based methods use network architectures such as convolutional autoencoders (Masci et al., 2011) or Generative Adversarial Networks (Goodfellow et al., 2014) to learn the appearance of anomaly-free samples. After training exclusively on such anomaly-free data their reconstructions during inference erase the defects in the anomalous test data. Consequently, comparing the input image with its reconstruction results in large deviations that indicate the presence of an anomaly (Bergmann et al., 2019b; Akçay et al., 2019; Luo et al., 2023). Embedding-based methods try to model the distribution of normal images in a predefined latent space. During inference, images outside of this distribution are considered as anomalous (Roth et al., 2022; Defard et al., 2020; Cohen and Hoshen, 2020). Combinations of both approaches also exist such as student-teacher networks. Utilizing Knowledge Distillation (Hinton et al., 2015; Ba and Caruana, 2014) a student network learns to imitate the embedding of a pretrained teacher network on anomaly-free data. Consequently, at test time the student fails to imitate the teacher for data containing defects. The discrepancy in the output of the two networks is used to detect the anomalies (Bergmann et al., 2020; Rudolph et al., 2023; Bergmann et al., 2022).

Pretrained Feature Extractors. Especially embedding-based and student-teacher approaches extensively make use of pretrained feature extractors to obtain distinctive features for anomaly-free and defective samples, respectively (Rippel et al., 2021; Reiss et al., 2021; Defard et al., 2020; Roth et al., 2022). These feature extractors such as ResNets (He et al., 2016), Wide ResNets (Zagoruyko and Komodakis, 2016), DenseNets (Huang et al., 2017) or EfficientNets (Tan and Le, 2019) are usually pretrained on large classification tasks like ImageNet (Krizhevsky et al., 2012) and remain fixed during training of the AD method. For instance, concatenating feature maps of different hierarchy levels of the extractor PaDiM (Defard et al., 2020) models the distribution of normal image patches by a multivariate Gaussian. Similarly, Cohen and Hoshen (2020) retrieve features on image level and use k-nearest-neighbors to determine the average distance of the test image to the normal training data. The state-of-the-art method PatchCore (Roth et al., 2022) creates a feature memory bank by subsampling the overall set of normal patch-features with a coreset-selection strategy (Sener and Savarese, 2018). Again, the locally aware patch-features combine feature maps from multiple layers of the extractor. The distance of a test patch-feature to this nominal memory bank defines the scoring function for detecting and localizing anomalies.

Synthetic Defects for Unsupervised Anomaly Detection. The lack of defective samples for training AD systems has led to the development of various approaches to generate and exploit synthetic defects. CutPaste (Li et al., 2021) cuts random image patches from a defect-free image and pastes them into another one. Schlüter et al. (2022) expand this strategy by Poisson image editing (Pérez et al., 2003) and background segmentation to obtain synthetic anomalies with a more natural appearance. Subsequently, both of these synthetic defect generation techniques are integrated into a self-supervised learning framework. Synthetic defects on image level are also exploited to obtain more expressive features for the given AD task (Cao et al., 2023). Likewise, perturbations in the feature space are intended to reflect synthetic abnormalities as well (Zavrtanik et al., 2022; Liu et al., 2023b). These perturbations may be used to train an anomaly detection module to distinguish normal from anomalous features. (Zavrtanik et al., 2022). SimpleNet (Liu et al., 2023b) further first utilizes a dedicated feature adaption module before adding Gaussian noise to the already adapted features. Subsequently, a discriminator network learns to distinguish normal from anomalous features.

Feature Selection for Anomaly Detection. Whereas the ideal properties of a feature for the task of Anomaly Detection and Localization are straightforward to define – similar for images or image patches from the anomaly-free class but far off from this distribution for anomalous samples or patches – selecting such distinctive features from a pretrained feature extractor is a much more challenging problem. Therefore, concatenating feature maps from different hierarchy levels has become a prominent approach for building expressive features (Roth et al., 2022; Defard et al., 2020; Liu et al., 2023b; Yu et al., 2021). Here, fine-grained details from earlier layers are usually joined with the high-level abstraction capability of later layers. However, recent work demonstrates that features extracted from a single layer of the extractor can lead to comparable or even superior performance for state-of-the-art AD methods (Heckler et al., 2023), provided that these single-layer-features are selected individually for each application scenario.

In this paper, we follow this line of work and propose a feature selection strategy for unsupervised AD when only considering a single layer for extracting features. Here, opposed to Heckler et al. (2023) who theoretically evaluate the potential of choosing an application-specific feature layer, we present and validate a strategy that can be implemented in real-world applications. Besides, we provide more fine-grained insights into the importance of feature selection by considering a substantially larger set of layers to choose from. To the best of our knowledge, we are the first to propose such a feature selection strategy for the task of Anomaly Detection and Localization. Accordingly, apart from the practical benefit, our method may also serve as a baseline for future research in this field.

3 METHOD

For identifying the most expressive features for a specific AD scenario we first investigate whether certain layers can be excluded from the overall set of layers of a pretrained feature extractor to define the solution space (Sec. 3.1). Thereafter, the techniques used to generate synthetic defects for our selection strategy are explained in detail (Sec. 3.2). Finally, the proposed application-specific selection strategy that identifies the most suitable layer for feature extraction is described (Sec. 3.3).

3.1 Layers Extracting Expressive Features

Using features from pretrained feature extractors for the task of unsupervised AD allows for choosing from a wide range of potential features. In theory, the feature map $F \in \mathbb{R}^{H \times W \times C}$ generated by any layer L of the extractor might be useful for the given application. Commonly, features from earlier layers are assumed to provide too little abstraction of the characteristics of the input image, whereas layers from the end of the extractor might be biased towards the pretraining task such as ImageNet classification (Roth et al., 2022). To investigate whether these assumptions are valid we analyze the set of potential features for an AD application as follows. Given an AD scenario and a pretrained feature extractor $\mathcal{X}_{pre}$ consisting of n layers $\mathcal{L} = \{L_i\}_{i=1\dots n}$, we obtain the overall set of features $\mathcal{F}$ by forwarding the anomaly-free training images $\mathcal{S}_{AD,train}$ through $\mathcal{X}_{pre}$ and extracting the features of every layer $L_i \in \mathcal{L}$, such that

$$\mathcal{F} = \{F_i | F_i = \mathcal{X}_{pre,i}\left(\mathcal{S}_{AD,train}\right), i = 1, \dots, n\}. \quad (1)$$

Here, $\mathcal{X}_{pre,i}$ defines the feature extraction of the i-th layer L_i in $\mathcal{X}_{pre}$. Considering only the features of a single layer we train the AD system with F_i and then evaluate the performance on the test set $\mathcal{S}_{AD,test}$. The

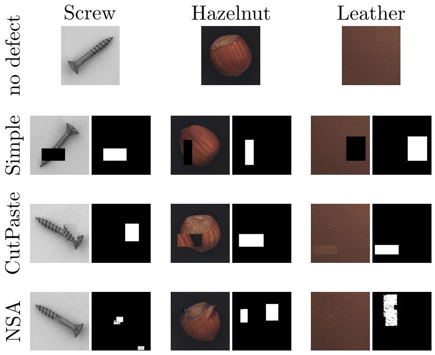

Figure 2: Synthetic defect types utilized within our feature selection strategy with corresponding ground truth maps.

features for the test set are extracted from the same layer $L_i \in \mathcal{L}$ of X_{pre} as for $\mathcal{S}_{AD,train}$.

Overall, by this fine-grained pre-analysis we explore whether it is possible to reduce the initial set of features to $\mathcal{F}_{red} \subseteq \mathcal{F}$ based on certain attributes of the corresponding layers such as the layer type or its position within the extractor network. Accordingly, the layers $\mathcal{L}_{red} \subseteq \mathcal{L}$ generating these features represent the set of layers to choose from for our feature selection strategy (Sec. 3.3).

3.2 Synthetic Defect Generation

The generation of synthetic defects has become a technique widely used in the domain of unsupervised AD (Cao et al., 2023; Zavrtanik et al., 2021; Guo et al., 2023; Zhang et al., 2023). We propose to exploit this technique for feature selection. In particular, we generate three different kinds of synthetic anomalies.

Simple Synthetic Anomalies. Given an anomaly-free image $x_{good} \in \mathbb{R}^{H\times W\times C}$ we randomly determine an axis-aligned rectangular region of size $H_{rand} \times W_{rand}$ that fits the original image dimensions. Then, the pixel values inside this region are set to 0 in every channel C of the image x_{good} to obtain the image containing the simple synthetic defect $x_{bad,syn}$. Visually, this results in a black rectangular area as shown in Fig. 2.

CutPaste for Synthetic Anomalies. Inspired by Li et al. (2021) we build upon their proposed CutPaste strategy to obtain images with artificial defects. Here, a region from an anomaly-free source image $x_{good,src}$ is cut out and the resulting crop is pasted into an anomaly-free target image $x_{good,tar}$ to obtain $x_{bad,syn}$. Both the size and position of the crop in the source image and the paste position in the target image are chosen randomly and independently from one another. Figure 2 illustrates some synthetic anomalies obtained through CutPaste.

Natural Synthetic Anomalies (NSA). In order to create synthetic defects with a more realistic appearance than the Simple or CutPaste defects we make use of a technique proposed by Schlüter et al. (2022). Here, random crops from the anomaly-free source image are scaled before pasting them into the anomaly-free target image. To obtain a more seamless blending Poisson image editing (Pérez et al., 2003) is utilized. Besides, a threshold operation is applied to $x_{good,src}$ and $x_{good,tar}$ that is intended to separate the object from the background. The crop and paste positions need to be inside the foreground region. Thus, the synthetic defects are likely to appear on the actual object and seem more natural (Fig. 2). The implementation of NSA also allows multiple defective regions in $x_{good,tar}$ in contrast to the other two defect types, where we only generate one anomalous region in the image.

3.3 Feature Selection Using Synthetic Defects

Given a set of layers $\mathcal{L}$ of the pretrained feature extractor X_{pre}, the task of feature selection is to identify the layer L^* which generates the optimal features for a specific AD scenario. Here, we consider the optimal layer L^* as the layer leading to the best AD performance when using its corresponding feature maps as extracted features. Feature selection can thus be formalized as $L^* = \text{select}(\mathcal{L})$ (Heckler et al., 2023).

We propose to utilize synthetic defects for defining the select-function (Fig. 3). In particular, we split the anomaly-free training set of an AD scenario $\mathcal{S}_{AD,train}$ into two disjoint parts $\mathcal{D}_T$ and $\mathcal{D}_V$. The first part $\mathcal{D}_T$ remains unchanged for training the AD system, whereas the second part $\mathcal{D}_V$ is split again disjointly into $\mathcal{D}_{V1}$ and $\mathcal{D}_{V2}$. Both $\mathcal{D}_{V1}$ and $\mathcal{D}_{V2}$ still only contain anomaly-free images. Now, the images in $\mathcal{D}_{V2}$ are augmented with synthetic defects, such that $\mathcal{D}_{V2}$ becomes $\mathcal{D}_{V,bad}$. For ease of notation we accordingly denote $\mathcal{D}_{V1}$ as $\mathcal{D}_{V,good}$. In total we thus obtain three non-overlapping dataset splits $\mathcal{D}_T$, $\mathcal{D}_{V,good}$ and $\mathcal{D}_{V,bad}$ from the original training set $\mathcal{S}_{AD,train}$. Using the features from a specific layer L the AD system is trained using $\mathcal{D}_T$. The trained model $\mathcal{M}_L$ is then evaluated on the union of $\mathcal{D}_{V,good}$ and $\mathcal{D}_{V,bad}$, the synthetic validation set $\mathcal{D}_{V,syn}$, with corresponding performance $\mathcal{P}\{\mathcal{M}_L(\mathcal{D}_{V,syn})\}$. The optimal layer L^* to be selected is the one maximizing $\mathcal{P}$:

$$L^* = \text{select}(\mathcal{L}) = \underset{L\in\mathcal{L}}{\arg\max}\, \mathcal{P}\{\mathcal{M}_L(\mathcal{D}_{V,syn})\} \qquad (2)$$

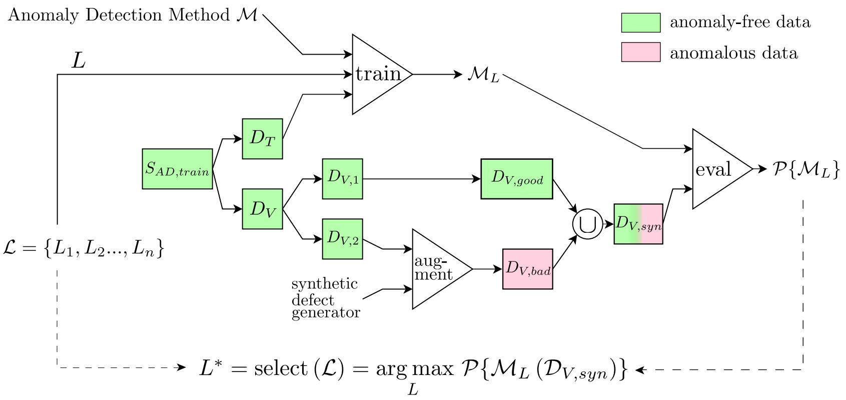
Anomaly Detection Method $\mathcal{M}$
🟩 anomaly-free data
🟥 anomalous data
L
train
$\mathcal{M}_L$
D_T
$S_{AD,train}$
$D_{V,1}$
$D_{V,good}$
D_V
$D_{V,2}$
aug-ment
$D_{V,bad}$
$\bigcup$
$D_{V,syn}$
eval
$\mathcal{P}\{\mathcal{M}_L\}$
$\mathcal{L} = \{L_1, L_2 ..., L_n\}$
synthetic defect generator
$L^* = \text{select}\,(\mathcal{L}) = \arg\max_{L}\, \mathcal{P}\{\mathcal{M}_L\,(\mathcal{D}_{V,syn})\}$

Figure 3: Feature Selection for Anomaly Detection. From the original training set $\mathcal{S}_{AD,train}$ a validation set $\mathcal{D}_V$ and training set $\mathcal{D}_T$ are created. A part of $\mathcal{D}_V$ is augmented with synthetic defects to obtain the synthetic validation set $\mathcal{D}_{V,syn}$ that contains both anomalous and anomaly-free images. The selected layer L^* is the layer leading to the best performance on $\mathcal{D}_{V,syn}$ when using its corresponding features for training the feature-extraction based AD method $\mathcal{M}$.

We assume that the features of the layer selected based on synthetic defects are also expressive for detecting defects that occur in real-world applications and, consequently, lead to high AD performance of the corresponding model $\mathcal{M}_{L^*}$.

4 EXPERIMENTS AND RESULTS

In this section we analyze the applicability of our proposed feature selection strategy. Generally, the model $\mathcal{M}_{L^*}$ using the features of the layer L^* selected without any real defective sample is evaluated on real test datasets $\mathcal{D}_{test}$. For this, we first describe the implementation details of our experiments, the used datasets and evaluation metrics. Then, we conduct a pre-analysis on the performance of layers to identify the solution space (Sec. 4.1) for our main experiment that validates the proposed selection strategy (Sec. 4.2). Further, we compare our single-layer results to multi-layer state-of-the-art performance (4.3) and provide ablation studies on e.g. the selection criterion (Sec. 4.4).

Implementation Details. In our experiments we consider two different methods for unsupervised AD: PatchCore (Roth et al., 2022) and SimpleNet (Liu et al., 2023b). While PatchCore directly uses the extracted features from a pretrained feature extractor to model the feature space without any further training, SimpleNet tries to adapt these features for the present AD task to the target domain. As feature extractors we investigate the widely used Wide ResNet-50 (Zagoruyko and Komodakis, 2016) and DenseNet-201 (Huang et al., 2017). Since each layer might provide expressive features for the given AD task (Sec. 4.1), we cannot discard any layer in advance and train both methods for each layer of those networks ($\mathcal{L}_{red} \equiv \mathcal{L}$). For extracting features, we use the feature extraction package[1] of torchvision in PyTorch (Paszke et al., 2019). This results in analyzing 172 layers for Wide ResNet-50 and 708 layers for DenseNet-201. We use the official implementations of PatchCore[2] and SimpleNet[3]. In the PatchCore implementation we fix the size of the coreset to 1000. We train SimpleNet for 160 epochs and report the result of the final model. For both methods we zoom input images to 256 × 256 spatial dimensions without center cropping.

Datasets. We train and evaluate individually on all 15 object categories of the MVTec AD dataset (Bergmann et al., 2019a). For the synthetic anomaly generation, we split the original train split $\mathcal{S}_{AD,train}$ of each dataset category into a train ($\mathcal{D}_T$) and a validation split ($\mathcal{D}_V$) that contain 70% and 30% of the original training images, respectively. Of the validation split $\mathcal{D}_V$ 75% of the images are modified to contain synthetic anomalies ($\mathcal{D}_{V,bad}$) and the remaining 25% of the images are not changed ($\mathcal{D}_{V,good}$). This good to bad ratio approximates the ratio in the real test set but remains constant for each object category.

Evaluation Metrics. In our experiments we evaluate both the quality of anomaly detection and anomaly localization. For anomaly detection on image-level we report the area under the receiver operator characteristic curve (AU-ROC). For anomaly localization on

[1] pytorch.org/vision/stable/feature_extraction.html

[2] github.com/amazon-science/patchcore-inspection

[3] github.com/DonaldRR/SimpleNet

pixel-level we use the area under per-region-overlap curve (AU-PRO) (Bergmann et al., 2019a). As suggested by Bergmann et al. (2019a) we integrate the PRO-curve only up to a false positive rate of 0.3 (AU-PRO$_{0.30}$) using the official evaluation code[4]. On image-level, we report the full area (AU-ROC$_{1.00}$).

Heckler et al. (2023) showed that distinct feature layers may be optimal for the respective task, detection and localization. However, considering real-world applicability we want to select a layer that solves both tasks adequately. Therefore, we compute the harmonic mean $\mathcal{P}_h$ of AU-ROC$_{1.00}$ and AU-PRO$_{0.30}$ and use this metric as performance measure

$$\mathcal{P}_h = \frac{2 \cdot \text{AU-ROC}_{1.00} \cdot \text{AU-PRO}_{0.30}}{\text{AU-ROC}_{1.00} + \text{AU-PRO}_{0.30}}. \qquad (3)$$

The harmonic mean heavily penalizes if one of the performance metrics is small and the other one is large, in contrast to the arithmetic mean (Komić, 2011). In real-world applications, achieving satisfactory results on both classifying and localizing anomalies is a vital characteristic of an AD system.

4.1 Can We Reduce the Initial Set of Layers?

In order to analyze whether it is possible to reduce the initial set of layers and, thus, features to choose from, we first group all available layers of a feature extractor according to their hierarchical position within the extractor and their layer type. Exemplary shown for MVTec AD object *grid* when using PatchCore with a Wide ResNet-50 feature extractor, at first glance the results in Figure 4a indicate that later layers containing higher-level semantics have the tendency to perform slightly worse than earlier layers or even layers from the input block. However, as shown in the appendix, these patterns vary significantly for different object categories. Likewise, patterns obtained by grouping the feature performances by their corresponding layer type are also very object-specific. In addition, even for one object category we can observe that features from any layer type might lead to high performance (Fig. 4b).

Heckler et al. (2023) hypothesized that a preselection of suitable layers based on the relative receptive field size might be possible. Therefore, we also determine the effective receptive field size (Luo et al., 2016) of each layer and divide it by the input image size to obtain this attribute. Figure 5 shows the AD performance over the relative receptive field size for PatchCore and both analyzed feature extractors, averaged over all 15 MVTec AD objects. Though an optimal range of the receptive field size seems to exist here in general, the performance variations within this range are still too large to use this attribute as a preselection criterion. Moreover, the potentially ideal range not only changes for distinct feature extractors but also varies significantly when using other methods such as SimpleNet, as shown in the appendix.

Considering all results from our extensive preanalysis we find that it is not possible to reduce the initial set of all layers $\mathcal{L}$ based on the analyzed layer attributes. Too many variations for distinct object-categories, feature extractors and AD methods occur. Therefore, rather than defining application-specific pre-selection criteria we developed a universal feature selection strategy that can cope with all these challenges to a certain extend, as presented within the next section.

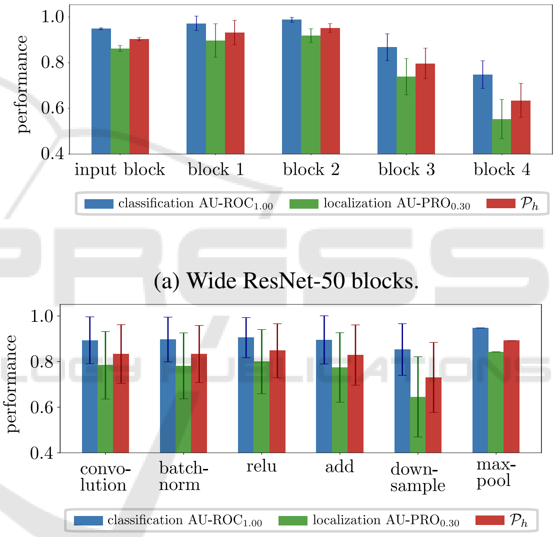

(a) Wide ResNet-50 blocks.

(b) Layer type.

Figure 4: AD metrics on real test set of MVTec AD object *grid*. Shown is for each metric the mean with standard deviation over all layers belonging to same block (a) and all layers of same type (b) in Wide ResNet-50, trained with PatchCore.

4.2 Feature Selection Using Synthetic Defects

Our proposed feature selection strategy is based on synthetic defects. We generate three different types of synthetic defects, namely *Simple*, *CutPaste* and *Natural Synthetic Anomalies (NSA)*, becoming more and more complex and realistic in this order. The idea is to transfer the AD performance from the synthetic to real data. For each defect type we select the layer L^* for which the model performs best on the syn-

[4] mvtec.com/company/research/datasets/mvtec-ad

Table 1: Harmonic mean $\mathcal{P}_h$ of AU-ROC$_{1.00}$ and AU-PRO$_{0.30}$ on the real test set of MVTec AD for the selected layers of each defect type. The last column *baseline* is the average performance of all layers. For each object, feature extractor and anomaly detection method, the best result is marked in bold.

	PatchCore								SimpleNet			
	WideResNet50				DenseNet201				WideResNet50			
object	Simple	CutPaste	NSA	baseline	Simple	CutPaste	NSA	baseline	Simple	CutPaste	NSA	baseline
bottle	88.4 ± 0.9	94.1 ± 0.8	**98.0** ± 0.2	91.0 ± 0.2	94.0 ± 0.2	95.0 ± 0.2	**97.4** ± 0.3	90.9 ± 0.0	74.4 ± 22.2	91.0 ± 0.4	**93.8** ± 0.7	42.8 ± 1.3
cable	77.1 ± 23.1	93.2 ± 1.2	**93.9** ± 1.1	81.3 ± 0.2	93.5 ± 1.9	93.9 ± 0.8	**94.7** ± 0.3	83.4 ± 0.1	47.7 ± 9.6	80.5 ± 2.1	**87.9** ± 0.7	38.0 ± 0.5
capsule	97.4 ± 0.4	91.7 ± 0.5	**97.5** ± 0.5	87.3 ± 0.1	90.8 ± 4.7	89.1 ± 1.3	**92.6** ± 2.7	81.2 ± 0.1	85.5 ± 2.2	**91.3** ± 1.5	77.8 ± 6.9	35.6 ± 0.6
carpet	73.1 ± 4.5	89.2 ± 8.0	**90.2** ± 1.5	89.8 ± 0.1	80.5 ± 9.7	**94.7** ± 0.8	85.7 ± 6.7	89.6 ± 0.0	52.8 ± 19.9	**87.8** ± 0.4	81.3 ± 4.8	59.0 ± 0.2
grid	90.1 ± 1.3	84.9 ± 1.3	**97.8** ± 0.8	83.7 ± 0.3	**97.7** ± 0.3	87.3 ± 3.2	97.4 ± 0.8	71.1 ± 0.3	36.9 ± 7.4	80.7 ± 0.6	**85.0** ± 2.2	28.4 ± 1.2
hazelnut	85.4 ± 7.5	96.3 ± 0.3	**97.4** ± 0.1	93.9 ± 0.2	96.9 ± 0.2	95.8 ± 0.4	**97.3** ± 0.1	91.9 ± 0.1	62.6 ± 4.1	86.9 ± 2.1	**89.1** ± 3.5	33.7 ± 0.5
leather	92.2 ± 1.3	96.6 ± 0.7	**98.9** ± 0.4	96.4 ± 0.0	**99.2** ± 0.1	97.8 ± 0.0	98.9 ± 0.0	95.3 ± 0.0	71.1 ± 9.2	95.9 ± 1.8	**98.1** ± 0.3	71.1 ± 0.4
metal nut	55.8 ± 14.4	90.1 ± 4.0	**96.0** ± 1.3	86.4 ± 0.2	90.9 ± 0.1	92.3 ± 0.7	**96.6** ± 0.8	85.4 ± 0.1	68.5 ± 16.2	88.6 ± 2.5	**91.5**± 0.4	35.2 ± 0.9
pill	**95.1** ± 1.1	88.4 ± 3.4	86.0 ± 7.9	85.4 ± 0.2	**90.4** ± 0.2	86.2 ± 2.6	79.2 ± 10.3	78.1 ± 0.0	74.9 ± 15.2	**83.5** ± 3.7	72.5 ± 11.1	32.7 ± 0.4
screw	59.2 ± 26.2	**82.7** ± 2.6	82.1 ± 11.9	72.0 ± 1.0	**81.0** ± 1.0	73.5 ± 1.8	76.5 ± 2.1	62.9 ± 0.5	0.2 ± 0.2	**73.0** ± 11.2	54.8 ± 18.5	28.5 ± 1.1
tile	87.5 ± 3.1	84.4 ± 1.5	**97.6** ± 0.0	88.6 ± 0.0	83.4 ± 2.2	**88.3** ± 4.3	84.0 ± 0.2	85.1 ± 0.0	20.1 ± 5.6	81.4 ± 3.8	**88.3** ± 4.6	55.1 ± 1.0
toothbrush	**94.0** ± 1.0	83.6 ± 1.4	89.7 ± 1.8	85.7 ± 0.1	**91.7** ± 0.3	86.2 ± 1.2	67.3 ± 2.7	81.7 ± 0.3	45.7 ± 8.4	**69.9** ± 0.8	68.5 ± 8.8	45.7 ± 1.3
transistor	58.3 ± 19.0	**95.8** ± 0.2	86.1 ± 3.4	80.9 ± 0.2	79.7 ± 7.3	**96.9** ± 0.2	88.6 ± 3.9	86.9 ± 0.2	43.8 ± 8.7	93.3 ± 0.5	**93.7** ± 0.1	35.7 ± 0.7
wood	93.0 ± 0.7	91.0 ± 1.4	**95.8** ± 0.3	88.3 ± 0.0	**94.3** ± 0.2	88.8 ± 0.3	89.4 ± 0.0	80.6 ± 0.0	35.9 ± 16.4	**82.8** ± 1.7	68.5 ± 13.3	53.1 ± 1.3
zipper	89.7 ± 2.2	94.8 ± 0.6	**96.7** ± 0.5	90.5 ± 0.0	93.4 ± 0.5	95.6 ± 0.4	**96.4** ± 0.5	88.5 ± 0.1	45.3 ± 9.1	88.7 ± 0.8	**95.0** ± 0.3	40.4 ± 0.7
mean	82.4 ± 11.2	90.4 ± 2.7	**93.6** ± 3.9	86.7 ± 0.3	90.5 ± 3.5	**90.8** ± 1.7	89.5 ± 3.5	83.5 ± 0.2	51.0 ± 12.0	**85.0** ± 3.5	83.1 ± 7.4	42.3 ± 0.9

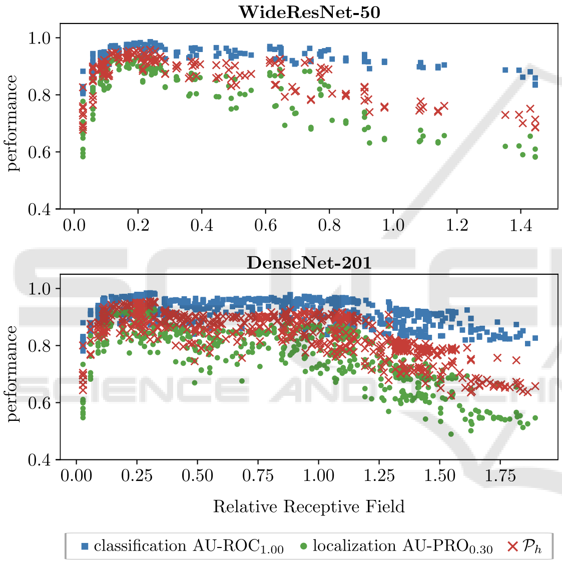

Figure 5: AD performance on the real test set over relative receptive field size of all layers of Wide ResNet-50 and DenseNet-201 when using the corresponding features for PatchCore. The mean values over all 15 MVTec AD objects are reported.

thetic validation set $\mathcal{D}_{V,syn}$ in terms of the harmonic mean $\mathcal{P}_h$ of AU-ROC$_{1.00}$ and AU-PRO$_{0.30}$. In Table 1 we report this metric of the chosen layer on the real test set $\mathcal{P}_h\{\mathcal{M}_{L^*}(\mathcal{D}_{test})\}$. We run PatchCore three times in each case. SimpleNet is run three times for Wide ResNet-50 but only once for DenseNet-201 due to the large number of layers and thus long training time. The results for SimpleNet with DenseNet-201 can be found in the appendix. The repeated experiments each have a different dataset split $\mathcal{D}_T$ and $\mathcal{D}_V$ and different generated synthetic anomalies in $\mathcal{D}_{V,bad}$. The reported values are the means of the three runs and the resulting standard deviations. Table 1 also contains a column *baseline*. We compute the baseline value $\mathcal{P}_b$ as average performance over all available layers $\mathcal{P}_b = \frac{1}{n}\sum_{l=1}^{n} \mathcal{P}_h\{\mathcal{M}_l(\mathcal{D}_{test})\}$ since this would be the expected value of $\mathcal{P}_h$ when choosing a random layer of the feature extractor.

In all experiments our feature selection method outperforms the baseline when using *CutPaste* or *NSA* defects. Even the very basic defect type *Simple* leads to a layer choice that benefits final performance on the real test set for many objects. As expected, the more realistic the defect types appear, the better performs the feature selection algorithm. For PatchCore the layer selection based on *NSA* outperforms the baseline by approximately 7 percentage points on average both for Wide ResNet-50 and DenseNet-201. The average performance of *Simple* defects is on par with those from *CutPaste* and *NSA* for DenseNet-201. It is significantly worse for Wide ResNet-50.

This could be due to the significantly larger standard deviations between different runs, compared to

Table 2: Performance ($\mathcal{P}_h$) on the real test set of MVTec AD of the layer L^* obtained by feature selection (FS) using *NSA* synthetic defects compared to using features concatenated from multiple layers (ML), both averaged over three runs.

	PatchCore				SimpleNet	
	WideResnet50		DenseNet201		WideResnet50	
object	FS	ML	FS	ML	FS	ML
bottle	**98.0** ± 0.2	97.8 ± 0.0	97.4 ± 0.3	**97.9** ± 0.1	**93.8** ± 0.7	71.4 ± 13.8
cable	93.9 ± 1.1	**94.5** ± 0.1	94.7 ± 0.3	**95.3** ± 0.2	**87.9** ± 0.7	73.8 ± 8.4
capsule	**97.5** ± 0.5	97.4 ± 0.2	92.6 ± 2.7	**96.5** ± 0.5	77.8 ± 6.9	**87.0** ± 5.1
carpet	90.2 ± 1.5	**96.4** ± 0.1	85.7 ± 6.7	**95.8** ± 0.3	**81.3** ± 4.8	69.6 ± 23.8
grid	**97.8** ± 0.8	96.0 ± 0.5	**97.4** ± 0.8	95.7 ± 0.7	**85.0** ± 2.2	34.7 ± 13.9
hazelnut	97.4 ± 0.1	**98.0** ± 0.2	**97.3** ± 0.1	**97.3** ± 0.3	**89.1** ± 3.5	35.5 ± 39.1
leather	98.9 ± 0.4	**99.0** ± 0.0	98.9 ± 0.0	**99.0** ± 0.0	**98.1** ± 0.3	94.5 ± 2.9
metal nut	96.0 ± 1.3	**97.3** ± 0.1	96.6 ± 0.8	**97.2** ± 0.1	**91.5** ± 0.4	67.7 ± 33.5
pill	86.0 ± 7.9	**96.2** ± 0.2	79.2 ± 10.3	**96.2** ± 0.2	72.5 ± 11.1	**88.2** ± 1.0
screw	82.1 ± 11.9	**94.4** ± 0.7	76.5 ± 2.1	**90.8** ± 1.5	**54.8** ± 18.5	14.1 ± 10.8
tile	**97.6** ± 0.0	94.6 ± 0.2	84.0 ± 0.2	**94.7** ± 0.1	**88.3** ± 4.6	41.0 ± 20.5
toothbrush	89.7 ± 1.8	**90.8** ± 0.0	67.3 ± 2.7	**91.8** ± 0.6	**68.5** ± 8.8	63.6 ± 4.0
transistor	86.1 ± 3.4	**89.5** ± 0.7	88.6 ± 3.9	**89.5** ± 0.2	**93.7** ± 0.1	84.4 ± 4.3
wood	**95.8** ± 0.3	95.0 ± 0.1	89.4 ± 0.0	**94.9** ± 0.2	**68.5** ± 13.3	65.2 ± 4.3
zipper	96.7 ± 0.5	**97.6** ± 0.1	96.4 ± 0.5	**97.7** ± 0.2	**95.0** ± 0.3	46.8 ± 16.5
mean	93.6 ± 3.9	**95.6** ± 0.3	89.5 ± 3.5	**95.4** ± 0.5	**83.1** ± 7.4	62.5 ± 17.5

those of *CutPaste* and *NSA*. The defect type *Simple* may give a good result with our feature selection method, but is clearly more unstable. The reason for this variability could be the large difference between the *Simple* defects, which are only black rectangles, and the real defects.

Looking at SimpleNet, there is a huge gap between the baseline performance and the performance of the feature selection based on *CutPaste* or *NSA*. Our proposed method outperforms the baseline by more than 40 percentage points, i.e. doubling the performance. Defect type *Simple* falls behind this performance, but is still 9 percentage points better than the baseline.

4.3 Comparison to Multi-Layer Features

Table 2 compares the performance of PatchCore and SimpleNet using multi-layer features as suggested in the original work (Roth et al., 2022; Liu et al., 2023b) to the results obtained by our feature selection using *NSA* defects. For both feature extractors the default multi-layer features are obtained by concatenating the feature maps of the last layers of block 2 and 3, respectively. On average, the selection of a single layer by our method provides slightly worse features for PatchCore than the default multi-layer setting. However, for most object categories feature selection leads to comparable results (e.g. Wide ResNet-50: objects cable, leather, toothbrush) or even outperforms the multi-layer baseline (e.g. Wide ResNet-50: objects bottle, capsule, tile). Likewise, for SimpleNet feature selection leads to significantly better results than the multi-layer setting for nearly all object categories. Compared to the original publication (Liu et al., 2023b) the multi-layer results for SimpleNet are significantly worse. This might be due to several reasons: We disable checkpoint selection based on the test set metrics, use a smaller number of training images and often the poor localization performance heavily affects the reported $\mathcal{P}_h$. In total, Table 2 not only verifies the feasibility of application-specific feature selection but also confirms its potential benefits over state-of-the-art default feature layers.

4.4 Ablation Studies

Choice of Selection Criterion. In Sec. 4.2 we select the layer L^* based on the best value of the harmonic mean $\mathcal{P}_h$ of AU-ROC$_{1.00}$ and AU-PRO$_{0.30}$ achieved on the synthetic validation set $\mathcal{D}_{V,syn}$. We want to investigate the impact of this selection criterion on the final performance on the real test set $\mathcal{D}_{test}$. Thus, we additionally perform feature layer selection based on anomaly classification performance $\mathcal{P}_{cls} =$ AU-ROC$_{1.00}$ and report all metrics in Table 3. The average performance over the three distinct dataset splits with synthetic defects of type *NSA*, exemplarily for PatchCore and DenseNet-201, is reported. We see that the layer selection outperforms the baseline for both selection criteria, and for all three evaluation metrics. As expected, the evaluation metric $\mathcal{P}_h$ on the real test data is higher when selecting the layer based on this metric (first column), than when selecting it based on $\mathcal{P}_{cls}$ (second column). Interestingly, even $\mathcal{P}_{cls}$ is higher in the former case. This means, that for the transfer from synthetic to real defective data it is important to select features that are distinctive for both anomaly classification and anomaly localization. This is in line with our motivation to also locate defects precisely in real-world applications.

Table 3: Comparison of average performances $\mathcal{P}_h$, $\mathcal{P}_{cls}$ and $\mathcal{P}_{loc}$ on the real test set of MVTec AD for feature layer selection by harmonic mean $\mathcal{P}_h$ and $\mathcal{P}_{cls}$ with the baseline. This table shows results of PatchCore on DenseNet-201 with feature selection based on defect type *NSA*.

selection crit.	Harmonic mean			AU-ROC$_{1.00}$			baseline		
object	$\mathcal{P}_h$	$\mathcal{P}_{cls}$	$\mathcal{P}_{loc}$	$\mathcal{P}_h$	$\mathcal{P}_{cls}$	$\mathcal{P}_{loc}$	$\mathcal{P}_h$	$\mathcal{P}_{cls}$	$\mathcal{P}_{loc}$
bottle	**97.4**	99.9	95.0	83.7	98.9	72.6	90.9	99.6	84.0
cable	**94.7**	99.0	90.9	86.3	95.4	78.8	83.4	92.0	76.9
capsule	**92.6**	95.7	89.8	82.5	89.7	76.5	81.2	89.5	75.0
carpet	85.7	85.4	85.9	**93.6**	97.3	90.2	89.6	95.0	85.1
grid	**97.4**	99.4	95.5	84.1	91.0	78.1	71.1	79.9	64.6
hazelnut	**97.3**	100.0	94.8	96.5	99.9	93.3	91.9	96.5	87.9
leather	**98.9**	100.0	97.8	97.0	100.0	94.2	95.3	99.0	92.1
metal nut	**96.6**	99.5	93.9	82.3	93.4	73.7	85.4	93.8	78.9
pill	**79.2**	87.6	73.5	75.6	81.3	70.8	78.1	83.5	74.0
screw	76.5	85.0	69.8	**84.2**	88.3	81.0	62.9	76.7	55.0
tile	84.0	95.6	74.9	**91.9**	99.4	85.5	85.1	98.0	75.5
toothbrush	67.3	84.8	55.9	73.4	93.3	60.5	**81.7**	93.2	73.5
transistor	88.6	99.2	80.2	**95.2**	99.0	91.7	86.9	94.9	80.7
wood	**89.4**	97.0	82.8	**89.4**	97.0	82.8	80.6	96.9	70.1
zipper	**96.4**	97.7	95.2	83.8	94.7	75.7	88.5	96.0	82.6
mean	**89.5**	95.1	85.1	86.6	94.6	80.4	83.5	92.3	77.1

Generalization from Synthetic to Real Data. To verify the generalization of feature selection using synthetic defects on real test data, Table 4 reports not only the performance on the real test set of the model using the features of the selected layer $\mathcal{M}_{L^*}$ $(k = 1)$ but also the averaged performance $\mathcal{P}_k = \frac{1}{k}\sum_{l=1}^{k} \mathcal{P}\{\mathcal{M}_l(\mathcal{D}_{test})\}$ over the top k layers with best performance on the synthetic validation set $\mathcal{D}_{V,syn}$. Especially for *NSA* synthetic defects the proposed selection strategy always outperforms the baseline of randomly choosing a single layer for *Metal Nut* and *Leather*. This indicates that the best features selected by our strategy using this kind of synthetic de-

Table 4: Average performance ($\mathcal{P}_h$) on the real test set of MVTec AD of the *k* best layers on the synthetic validation set for PatchCore with a Wide ResNet-50 feature extractor using different synthetic defects. Results are averaged over three distinct initial dataset splits $\mathcal{D}_T$ and $\mathcal{D}_V$ and compared to the average performance over all layers.

object	Metal Nut			Leather		
k	Simple	CutPaste	NSA	Simple	CutPaste	NSA
1	55.8 ± 0.0	90.1 ± 0.0	**96.0** ± 0.0	92.2 ± 0.0	96.6 ± 0.0	**98.9** ± 0.0
2	51.4 ± 16.4	91.4 ± 1.9	**96.1** ± 0.9	92.9 ± 0.8	96.7 ± 1.0	**98.9** ± 0.0
3	50.8 ± 14.2	91.4 ± 1.9	**96.2** ± 0.8	93.9 ± 1.6	96.4 ± 1.0	**99.0** ± 0.2
4	61.6 ± 22.6	90.5 ± 2.8	**96.4** ± 0.8	94.0 ± 1.4	96.8 ± 1.1	**98.8** ± 0.4
all	86.4 ± 12.8			96.4 ± 3.0		

fect consistently generalize well to the defects occurring in the real test set. This also applies to utilizing *CutPaste* defects, whereas *Simple* defects are both insufficient and less stable. The complete ablation is provided in the appendix.

5 CONCLUSION

Using features from a pretrained feature extractor has become a popular paradigm in developing methods for the task of unsupervised Anomaly Detection and Localization. Commonly, for different application scenarios features from the same layers are utilized. Moreover, oftentimes multiple feature maps are combined to obtain expressive features. However, recent work found that an optimal, application-specific selection of a single feature layer is sufficient to reach state-of-the-art performance or even outperforms the default multi-layer setting (Heckler et al., 2023).

In this paper, we followed this line of work and proposed the first feature selection strategy for AD. First, we demonstrated the necessity of considering all layers of a pretrained feature extractor in application-specific feature selection. Thereupon, we presented a selection strategy based on synthetic defects that chooses from this overall set of layers and does not require any real anomalous samples. Our proposed strategy was evaluated for two state-of-the-art AD methods, PatchCore (Roth et al., 2022) and SimpleNet (Liu et al., 2023b), as well as two feature extractors, Wide ResNet-50 (Zagoruyko and Komodakis, 2016) and DenseNet-201 (Huang et al., 2017), both pretrained on ImageNet (Krizhevsky et al., 2012). Especially using *CutPaste* or *NSA* synthetic defects for our selection strategy consistently led to improvements over the expected value of a randomly chosen layer. Moreover, for certain object categories of the MVTec AD dataset application-specific feature selection outperformed the default multi-layer features as well.

Overall, our method may serve as a competitive baseline for further research in this field. However, future work may reduce the computational cost of estimating the suitability of a layer for generating application-specific features. Other synthetic defect types may also be considered in combination with our strategy, potentially leading to an even more consistent improvement over ensembled features from multiple layers.

REFERENCES

Akçay, S., Atapour-Abarghouei, A., and Breckon, T. P. (2019). Skip-ganomaly: Skip connected and adversarially trained encoder-decoder anomaly detection. In *2019 International Joint Conference on Neural Networks (IJCNN)*, pages 1–8.

Ba, J. and Caruana, R. (2014). Do deep nets really need to be deep? In Ghahramani, Z., Welling, M., Cortes, C., Lawrence, N., and Weinberger, K., editors, *Advances in Neural Information Processing Systems*, volume 27. Curran Associates, Inc.

Bergmann, P., Batzner, K., Fauser, M., Sattlegger, D., and Steger, C. (2022). Beyond Dents and Scratches: Logical Constraints in Unsupervised Anomaly Detection and Localization. *International Journal of Computer Vision*, 130(4):947–969.

Bergmann, P., Fauser, M., Sattlegger, D., and Steger, C. (2019a). MVTec AD — A Comprehensive Real-World Dataset for Unsupervised Anomaly Detection. In *IEEE Conference on Computer Vision and Pattern Recognition (CVPR)*, pages 9584–9592.

Bergmann, P., Fauser, M., Sattlegger, D., and Steger, C. (2020). Uninformed Students: Student-Teacher Anomaly Detection With Discriminative Latent Embeddings. In *IEEE Conference on Computer Vision and Pattern Recognition (CVPR)*, pages 4182–4191.

Bergmann, P., Löwe, S., Fauser, M., Sattlegger, D., and Steger, C. (2019b). Improving Unsupervised Defect Segmentation by Applying Structural Similarity to Autoencoders. In *Proceedings of the 14th International Joint Conference on Computer Vision, Imaging and Computer Graphics Theory and Applications - Volume 5: VISAPP*, pages 372–380. INSTICC, SciTePress.

Blum, H., Sarlin, P.-E., Nieto, J., Siegwart, R., and Cadena, C. (2019). Fishyscapes: A Benchmark for Safe Semantic Segmentation in Autonomous Driving. In *IEEE International Conference on Computer Vision Workshops (ICCVW)*, pages 2403–2412.

Cao, Y., Xu, X., Liu, Z., and Shen, W. (2023). Collaborative discrepancy optimization for reliable image anomaly localization. *IEEE Transactions on Industrial Informatics*, pages 1–10.

Cohen, N. and Hoshen, Y. (2020). Sub-image anomaly detection with deep pyramid correspondences. *arXiv preprint arXiv:2005.02357v1*.

Cui, Y., Liu, Z., and Lian, S. (2023). A survey on unsupervised anomaly detection algorithms for industrial images. *IEEE Access*, 11:55297–55315.

Defard, T., Setkov, A., Loesch, A., and Audigier, R. (2020). Padim: A patch distribution modeling framework for anomaly detection and localization. In *Pattern Recognition. ICPR International Workshops and Challenges 2021, Proceedings, Part IV*, volume 12664 of *Lecture Notes in Computer Science*, pages 475–489. Springer.

Goodfellow, I., Pouget-Abadie, J., Mirza, M., Xu, B., Warde-Farley, D., Ozair, S., Courville, A., and Bengio, Y. (2014). Generative adversarial nets. In Ghahramani, Z., Welling, M., Cortes, C., Lawrence, N., and Weinberger, K., editors, *Advances in Neural Information Processing Systems*, volume 27. Curran Associates, Inc.

Guo, Y., Jiang, M., Huang, Q., Cheng, Y., and Gong, J. (2023). Mldfr: A multilevel features restoration method based on damaged images for anomaly detection and localization. *IEEE Transactions on Industrial Informatics*, pages 1–10.

He, K., Zhang, X., Ren, S., and Sun, J. (2016). Deep Residual Learning for Image Recognition. In *IEEE Conference on Computer Vision and Pattern Recognition (CVPR)*, pages 770–778.

Heckler, L., König, R., and Bergmann, P. (2023). Exploring the importance of pretrained feature extractors for unsupervised anomaly detection and localization. In *Proceedings of the IEEE/CVF Conference on Computer Vision and Pattern Recognition (CVPR) Workshops*, pages 2916–2925.

Hendrycks, D., Basart, S., Mazeika, M., Mostajabi, M., Steinhardt, J., and Song, D. (2019). A Benchmark for Anomaly Segmentation. *arXiv preprint arXiv:1911.11132v1*.

Hinton, G., Vinyals, O., and Dean, J. (2015). Distilling the knowledge in a neural network.

Huang, G., Liu, Z., van der Maaten, L., and Weinberger, K. Q. (2017). Densely connected convolutional networks. In *Proceedings of the IEEE Conference on Computer Vision and Pattern Recognition (CVPR)*.

Komić, J. (2011). Harmonic mean. In *International Encyclopedia of Statistical Science*, pages 622–624, Berlin, Heidelberg. Springer Berlin Heidelberg.

Krizhevsky, A., Sutskever, I., and Hinton, G. E. (2012). ImageNet Classification With Deep Convolutional Neural Networks. In *Advances in Neural Information Processing Systems*, pages 1097–1105.

Li, C.-L., Sohn, K., Yoon, J., and Pfister, T. (2021). Cutpaste: Self-supervised learning for anomaly detection and localization. In *2021 IEEE/CVF Conference on Computer Vision and Pattern Recognition (CVPR)*, pages 9659–9669.

Li, W.-X., Mahadevan, V., and Vasconcelos, N. (2013). Anomaly Detection and Localization in Crowded Scenes. *IEEE Transactions on Pattern Analysis and Machine Intelligence (TPAMI)*, 36(1):18–32.

Liu, J., Xie, G., Wang, J., Li, S., Wang, C., Zheng, F., and Jin, Y. (2023a). Deep industrial image anomaly detection: A survey. *arXiv preprint arXiv:2301.11514*.

Liu, Z., Zhou, Y., Xu, Y., and Wang, Z. (2023b). Simplenet: A simple network for image anomaly detection and localization. In *Proceedings of the IEEE/CVF Conference on Computer Vision and Pattern Recognition (CVPR)*, pages 20402–20411.

Luo, W., Li, Y., Urtasun, R., and Zemel, R. (2016). Understanding the effective receptive field in deep convolutional neural networks. In *Advances in Neural Information Processing Systems*, volume 29. Curran Associates, Inc.

Luo, W., Yao, H., and Yu, W. (2023). Normal reference attention and defective feature perception network for surface defect detection. *IEEE Transactions on Instrumentation and Measurement*, 72:1–14.

Masci, J., Meier, U., Cireşan, D., and Schmidhuber, J. (2011). Stacked Convolutional Auto-Encoders for Hierarchical Feature Extraction. In *Artificial Neural Networks and Machine Learning – ICANN 2011*, pages 52–59. Springer.

Menze, B. H., Jakab, A., Bauer, S., Kalpathy-Cramer, J., Farahani, K., Kirby, J., et al. (2015). The Multimodal Brain Tumor Image Segmentation Benchmark (BRATS). *IEEE Transactions on Medical Imaging*, 34(10):1993–2024.

Nazare, T. S., de Mello, R. F., and Ponti, M. A. (2018). Are pre-trained cnns good feature extractors for anomaly detection in surveillance videos? *arXiv preprint arXiv:1811.08495*.

Paszke, A., Gross, S., Massa, F., Lerer, A., Bradbury, J., Chanan, G., Killeen, T., Lin, Z., Gimelshein, N., Antiga, L., Desmaison, A., Kopf, A., Yang, E., DeVito, Z., Raison, M., Tejani, A., Chilamkurthy, S., Steiner, B., Fang, L., Bai, J., and Chintala, S. (2019). PyTorch: An Imperative Style, High-Performance Deep Learning Library. In *Advances in Neural Information Processing Systems*, volume 32.

Pérez, P., Gangnet, M., and Blake, A. (2003). Poisson image editing. *ACM Trans. Graph.*, 22(3):313–318.

Prunella, M., Scardigno, R. M., Buongiorno, D., Brunetti, A., Longo, N., Carli, R., Dotoli, M., and Bevilacqua, V. (2023). Deep learning for automatic vision-based recognition of industrial surface defects: A survey. *IEEE Access*, 11:43370–43423.

Reiss, T., Cohen, N., Bergman, L., and Hoshen, Y. (2021). Panda: Adapting pretrained features for anomaly detection and segmentation. In *Proceedings of the IEEE/CVF Conference on Computer Vision and Pattern Recognition*, pages 2806–2814.

Rippel, O., Mertens, P., and Merhof, D. (2021). Modeling the distribution of normal data in pre-trained deep features for anomaly detection. In *2020 25th International Conference on Pattern Recognition (ICPR)*. IEEE.

Roth, K., Pemula, L., Zepeda, J., Schölkopf, B., Brox, T., and Gehler, P. V. (2022). Towards total recall in industrial anomaly detection. In *IEEE/CVF Conference on Computer Vision and Pattern Recognition, CVPR 2022*, pages 14298–14308. IEEE.

Rudolph, M., Wehrbein, T., Rosenhahn, B., and Wandt, B. (2023). Asymmetric student-teacher networks for industrial anomaly detection. In *IEEE/CVF Winter Conference on Applications of Computer Vision, WACV 2023*, pages 2591–2601. IEEE.

Schlüter, H. M., Tan, J., Hou, B., and Kainz, B. (2022). Natural synthetic anomalies for self-supervised anomaly detection and localization. In Avidan, S., Brostow, G., Cissé, M., Farinella, G. M., and Hassner, T., editors, *Computer Vision – ECCV 2022*, pages 474–489, Cham. Springer Nature Switzerland.

Seeböck, P., Orlando, J. I., Schlegl, T., Waldstein, S. M., Bogunović, H., Klimscha, S., Langs, G., and Schmidt-Erfurth, U. (2020). Exploiting epistemic uncertainty of anatomy segmentation for anomaly detection in retinal oct. *IEEE Transactions on Medical Imaging*, 39(1):87–98.

Sener, O. and Savarese, S. (2018). Active learning for convolutional neural networks: A core-set approach. In *6th International Conference on Learning Representations, ICLR 2018*.

Tan, M. and Le, Q. (2019). Efficientnet: Rethinking model scaling for convolutional neural networks. In *International conference on machine learning*, pages 6105–6114. PMLR.

Yu, J., Zheng, Y., Wang, X., Li, W., Wu, Y., Zhao, R., and Wu, L. (2021). Fastflow: Unsupervised anomaly detection and localization via 2d normalizing flows. *arXiv preprint arXiv:2111.07677v2*.

Zagoruyko, S. and Komodakis, N. (2016). Wide residual networks. In *British Machine Vision Conference 2016*. British Machine Vision Association.

Zavrtanik, V., Kristan, M., and Skočaj, D. (2022). Dsr – a dual subspace re-projection network for surface anomaly detection. In Avidan, S., Brostow, G., Cissé, M., Farinella, G. M., and Hassner, T., editors, *Computer Vision – ECCV 2022*, pages 539–554, Cham. Springer Nature Switzerland.

Zavrtanik, V., Kristan, M., and Skočaj, D. (2021). Draem - a discriminatively trained reconstruction embedding for surface anomaly detection. In *Proceedings of the IEEE/CVF International Conference on Computer Vision (ICCV)*, pages 8330–8339.

Zhang, X., Li, S., Li, X., Huang, P., Shan, J., and Chen, T. (2023). Destseg: Segmentation guided denoising student-teacher for anomaly detection. In *Proceedings of the IEEE/CVF Conference on Computer Vision and Pattern Recognition (CVPR)*, pages 3914–3923.

Zou, Y., Jeong, J., Pemula, L., Zhang, D., and Dabeer, O. (2022). Spot-the-difference self-supervised pre-training for anomaly detection and segmentation. In *Computer Vision – ECCV 2022*, pages 392–408, Cham. Springer Nature Switzerland.

APPENDIX

Implementation Details of Synthetic Defects

For all three defect types $\mathcal{D}_{V,bad}$ consists of the same original images, only the synthetic defect type differs. We do not put any prior knowledge on the real defects into defect generation.

Simple and CutPaste. We parameterize the rectangles such that they have a minimum distance to the image borders of 20 pixels. Width and height are randomly sampled and cover between ten and fifty percent of the image width and height, respectively. Thus, it is not guaranteed that the defect appears on the actual object in the image.

Natural Synthetic Anomalies (NSA). We make use of the official implementation at https://github.com/hmsch/natural-synthetic-anomalies with commit id 9195916 and use all of the proposed parameters. In particular, we distinguish between objects and textures for the Poisson blending. *NSA* (Schlüter et al., 2022) also estimates the background to ensure that defects are generated on the objects. However, this procedure sometimes fails and defects can also occur in the background. In each image, the number of generated defects is randomly sampled between 1 and 4 for textures and objects *screw* and *zipper* and between 1 and 3 for the remaining objects.

Can We Reduce the Initial Set of Layers?

For the following experiments we trained on a reduced training set $\mathcal{D}_T$ of the original training set $\mathcal{S}_{AD,train}$ and evaluate the performance on the original test set $\mathcal{S}_{AD,test}$ for each MVTec AD object category, respectively. For comparability to our main experiments, $\mathcal{D}_T$ contains 70% of the original anomaly-free training images.

Performance by Block and Layer Type. The performance when exclusively using a single layer L for feature extraction grouped by block for MVTec AD object *cable* is provided in Figure A.1 for PatchCore. In contrast to object *grid* (Figure 4a), features from later layers are more suitable.

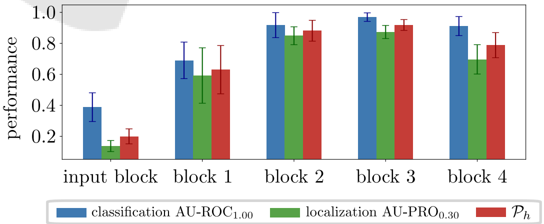

Figure A.1: AD metrics on real test set of MVTec AD object *cable*. Shown is for each metric the mean with standard deviation over all layers belonging to same block in Wide ResNet-50, trained with PatchCore.

Performance over Relative Receptive Field. The performance averaged over all MVTec AD objects for SimpleNet is shown in Figure A.2.

Table A.1: Average performance ($\mathcal{P}_h$) on the real test set of MVTec AD of the *k* best layers on the synthetic validation set for PatchCore with a Wide ResNet-50 feature extractor using different synthetic defects. Results are averaged over three distinct initial dataset splits $\mathcal{D}_T$ and $\mathcal{D}_V$ and compared to the average performance over all layers.

object	Bottle			Cable			Capsule			Hazelnut			Carpet		
k	Simple	CutPaste	NSA	Simple	CutPaste	NSA	Simple	CutPaste	NSA	Simple	CutPaste	NSA	Simple	CutPaste	NSA
1	88.4 ± 0.0	94.1 ± 0.0	**98.0** ± 0.0	77.1 ± 0.0	93.2 ± 0.0	**93.9** ± 0.0	97.4 ± 0.0	91.7 ± 0.0	**97.5** ± 0.0	85.4 ± 0.0	96.3 ± 0.0	**97.4** ± 0.0	73.1 ± 0.0	89.2 ± 0.0	**90.2** ± 0.0
2	72.8 ± 17.3	93.9 ± 0.4	**98.1** ± 0.1	77.5 ± 19.1	92.9 ± 1.1	**93.9** ± 0.7	97.2 ± 0.2	91.8 ± 0.4	**97.3** ± 0.2	88.7 ± 5.1	96.4 ± 0.1	**97.2** ± 0.2	71.5 ± 2.6	84.2 ± 6.2	**90.9** ± 1.0
3	77.3 ± 15.9	93.9 ± 0.7	**98.1** ± 0.2	82.8 ± 17.9	92.9 ± 1.0	**93.5** ± 1.0	91.1 ± 10.5	91.6 ± 0.5	**97.4** ± 0.3	89.3 ± 4.7	96.3 ± 0.3	**97.3** ± 0.3	69.0 ± 4.3	84.9 ± 5.6	**91.2** ± 1.3
4	77.5 ± 14.0	93.8 ± 0.8	**98.0** ± 0.2	85.1 ± 16.3	93.2 ± 1.0	**93.7** ± 0.9	92.7 ± 9.7	91.2 ± 1.4	**97.5** ± 0.3	90.9 ± 5.2	96.3 ± 0.6	**97.4** ± 0.3	74.3 ± 10.0	85.0 ± 10.3	**91.2** ± 1.3
all	91.0 ± 8.0			81.3 ± 16.9			87.3 ± 10.7			93.9 ± 5.4			89.8 ± 6.6		

object	Pill			Screw			Toothbrush			Transistor			Zipper		
k	Simple	CutPaste	NSA	Simple	CutPaste	NSA	Simple	CutPaste	NSA	Simple	CutPaste	NSA	Simple	CutPaste	NSA
1	**95.1** ± 0.0	88.4 ± 0.0	86.0 ± 0.0	59.2 ± 0.0	**82.7** ± 0.0	82.1 ± 0.0	**94.0** ± 0.0	83.6 ± 0.0	89.7 ± 0.0	58.3 ± 0.0	**95.8** ± 0.0	86.1 ± 0.0	89.7 ± 0.0	94.8 ± 0.0	**96.7** ± 0.0
2	**95.5** ± 0.9	89.8 ± 2.1	87.9 ± 2.4	59.2 ± 13.0	**82.4** ± 1.8	78.9 ± 7.8	**93.5** ± 1.0	85.0 ± 1.5	88.6 ± 1.5	66.9 ± 11.7	**95.8** ± 0.2	87.2 ± 3.1	88.4 ± 3.1	94.2 ± 0.6	**96.6** ± 0.4
3	**95.3** ± 0.8	90.4 ± 2.2	90.3 ± 5.3	64.6 ± 14.1	**82.9** ± 2.4	78.8 ± 7.3	**90.7** ± 5.2	85.4 ± 1.4	88.6 ± 1.5	65.9 ± 12.9	**95.9** ± 0.2	86.7 ± 2.7	86.4 ± 4.5	93.9 ± 1.0	**96.9** ± 0.8
4	**94.7** ± 1.7	90.0 ± 2.2	91.0 ± 5.6	65.4 ± 13.6	**83.2** ± 2.9	78.4 ± 6.4	**91.9** ± 5.1	85.0 ± 1.7	88.2 ± 1.5	67.0 ± 15.9	**95.9** ± 0.3	88.2 ± 3.5	85.6 ± 4.3	94.0 ± 0.9	**96.8** ± 0.9
all	85.4 ± 10.6			72.0 ± 18.6			85.7 ± 8.4			80.9 ± 15.3			90.5 ± 8.2		

object	Grid			Tile			Wood		
κ	Simple	CutPaste	NSA	Simple	CutPaste	NSA	Simple	CutPaste	NSA
1	90.1 ± 0.0	84.9 ± 0.0	**97.8** ± 0.0	87.5 ± 0.0	84.4 ± 0.0	**97.6** ± 0.0	93.0 ± 0.0	91.0 ± 0.0	**95.8** ± 0.0
2	90.6 ± 0.7	84.5 ± 0.6	**97.4** ± 0.5	86.9 ± 1.8	85.0 ± 2.3	**97.7** ± 0.1	92.7 ± 0.8	89.0 ± 2.7	**95.7** ± 0.3
3	90.3 ± 0.8	84.4 ± 0.5	**97.4** ± 0.5	89.1 ± 3.5	85.5 ± 2.3	**97.1** ± 0.9	92.8 ± 0.7	89.9 ± 3.0	**95.6** ± 0.3
4	89.4 ± 3.7	83.6 ± 1.6	**97.2** ± 0.8	89.7 ± 4.2	85.6 ± 2.2	**96.8** ± 1.0	92.7 ± 0.7	89.0 ± 3.0	**95.6** ± 0.4
all	83.7 ± 12.4			88.6 ± 6.5			88.3 ± 8.6		

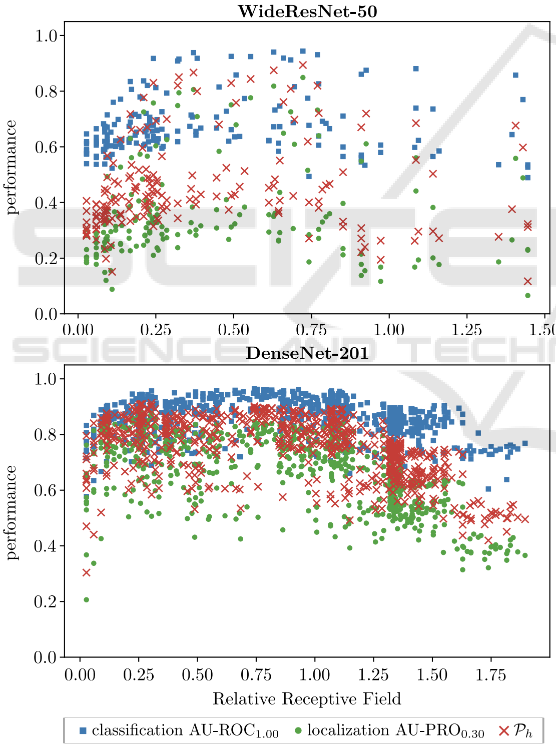

Figure A.2: AD performance on the real test set over relative receptive field size of all layers of Wide ResNet-50 and DenseNet-201 when using the corresponding features for SimpleNet. The mean values over all 15 MVTec AD objects are reported.

- Considering all experiments, the observed patterns vary significantly for different object categories and methods such that a universal pre-selection of expressive features by block, layer type or relative receptive field size is challenging.

Feature Selection Using Synthetic Defects

The results of our main experiment where we apply our feature selection strategy using different synthetic defects for SimpleNet extracting features with a single layer of a DenseNet-201 can be found in Table A.2.

Table A.2: Harmonic mean $\mathcal{P}_h$ on the real test set of MVTec AD for the selected layers of each defect type, for SimpleNet with a DenseNet-201 feature extractor. The last column *baseline* is the average performance of all layers. Only a single run was conducted.

object	Simple	CutPaste	NSA	baseline
bottle	94.2	93.0	**96.7**	87.0
cable	68.5	**92.7**	90.3	68.8
capsule	93.8	67.2	**94.1**	71.9
carpet	70.4	**91.5**	78.2	81.0
grid	97.0	88.3	**97.8**	67.2
hazelnut	93.7	96.3	**96.8**	79.1
leather	**99.1**	97.4	98.9	90.3
metal nut	86.1	92.3	**93.9**	73.9
pill	**89.4**	78.8	63.7	65.8
screw	**77.4**	73.9	60.0	55.4
tile	70.8	**86.3**	82.2	72.6
toothbrush	**84.5**	76.3	33.9	73.9
transistor	62.4	**95.8**	83.9	73.1
wood	84.9	84.4	**85.6**	70.6
zipper	95.5	95.4	**96.9**	83.7
mean	84.5	**87.3**	83.5	74.3

Ablation Studies

Generalization from Synthetic to Real Data. The results of all MVTec AD objects for our ablation study that validates the consistent generalization from synthetic to real defects in our selection strategy, especially for defect types *CutPaste* and *NSA*, can be found in Table A.1 for PatchCore extracting features with a single Wide ResNet-50 layer.